Night-time chemistry of biomass burning emissions in urban areas: A dual mobile chamber study

Spiro D. Jorga[1], Kalliopi Florou[2], Christos Kaltsonoudis[2], John K. Kodros[2], Christina Vasilakopoulou[2,3], Manuela Cirtog[5], Axel Fouqueau[6], Bénédicte Picquet-Varrault[5], Athanasios Nenes[2,4], and Spyros N. Pandis[1,2,3]

[1]Department of Chemical Engineering, Carnegie Mellon University, Pittsburgh, 15213, USA

[2]Institute of Chemical Engineering Sciences, ICE-HT, Patras, 26504, Greece

[3]Department of Chemical Engineering, University of Patras, Patras, 26504, Greece

[4]School of Architecture, Civil & Environmental Engineering, Ecole Polytechnique Federale de Lausanne, Lausanne, 1015, Switzerland

[5]LISA, UMR CNRS 7583, Université Paris-Est Créteil, Université de Paris, Institut Pierre Simon Laplace (IPSL), Créteil, France

[6]Laboratoire National de Métrologie et d'Essais (LNE), 75015 Paris, France

Correspondence to: Spyros N. Pandis (spyros@chemeng.upatras.gr)

Abstract

Residential biomass burning for heating purposes is an important source of air pollutants during winter. Here we test the hypothesis that significant secondary organic aerosol production can take place even during winter nights through oxidation of the emitted organic vapors by the nitrate (NO_3) radical produced during the reaction of ozone and nitrogen oxides. We use a mobile dual smog chamber system which allows the study of chemical aging of ambient air against a control reference. Ambient urban air sampled during a wintertime campaign during night-time periods with high concentrations of biomass burning emissions was used as the starting point of the aging experiments. Biomass burning organic aerosol (OA) was on average 70% of the total OA in the beginning of our experiments. Ozone was added in the perturbed chamber to simulate mixing with background air (and subsequent NO_3 radical production and aging), while the second chamber was used as a reference. Following the injection of ozone, rapid OA formation was observed in all experiments leading to increases of the OA concentration by 20-70%. The oxygen-to-carbon ratio of the OA increased on average by 50% and the mass spectra of the produced OA was quite similar to the oxidized OA mass spectra reported during winter in urban areas. Further, good correlation was found for the OA mass spectra between the ambient-derived emissions in this study and the nocturnal aged laboratory-derived biomass burning emissions from previous work. Concentrations

of NO_3 radicals as high as 25 ppt were measured in the perturbed chamber with an accompanying production of 0.1-3.2 µg m^{-3} of organic nitrate in the aerosol phase. Organic nitrate represented approximately 10% of the mass of the secondary OA formed. These results strongly indicate that the OA in biomass burning plumes can chemically evolve rapidly even during wintertime periods with low photochemical activity.

1. Introduction

Biomass burning from residential heating, agricultural fires, prescribed burning, and wildfires is a major source of atmospheric pollutants worldwide (Watson 2002, Bond et al. 2004, Robinson et al. 2006). Emissions from biomass burning contribute both primary organic aerosol (POA) and organic vapors that upon further reactions in the atmosphere can produce secondary organic aerosol (SOA) (Andreae & Merlet 2001, Akagi et al., 2011, Bruns et al., 2016, Akherati et al., 2020). The use of wood burning for domestic heating purposes is one of the major sources of OA in many countries and is a major contributor to the violation of daily PM standards in European cities (Alfarra et al., 2007, Favez et al., 2010, Fuller et al., 2014). Biomass burning emissions and their products have significant but still uncertain impacts on human health and climate (Ford et al., 2018; O'Dell et al., 2019).

The organic aerosol emitted during biomass burning undergoes extensive physical and chemical changes in the atmosphere. More volatile components evaporate as emissions dilute in the atmosphere (Tkacik et al., 2017); these semivolatile organic compounds (SVOCs) together with the other emitted intermediate volatility (IVOCs) and volatile organic compounds (VOCs) are subsequently oxidized leading to the production of SOA. Photochemical oxidation of biomass burning emissions and the resulting SOA production have been studied both in the laboratory (Hennigan et al., 2011; Ortega et al., 2013; Tkacik et al., 2017; Ahern et al.; 2019; Kodros et al., 2020) and in the field (Capes et al., 2008; Jolleys et al., 2015; Vakkari et al., 2018). The reactions of VOCs, IVOCs and SVOCs with the OH radical are considered to be the dominant chemical pathway for oxidation, but reactions of emitted monoterpenes with ozone can also contribute to the SOA formation during the chemical aging of biomass burning emissions (Yu et al., 1999, Zhao et al., 2015). Despite considerable uncertainties remaining on the amount of SOA that can be produced, and the net change of the biomass burning OA concentration when evaporation is

63 considered, it is clear that this daytime processing is important for converting the fresh biomass

64 burning OA to oxidized OA (OOA) (Bougiatioti et al., 2014).

65   Atmospheric processing of biomass burning OA during periods of low photochemical

66 activity (such as in winter or at night), known also as "dark" aging, has received substantially less

67 attention than photochemical processing. Recent aircraft measurements during agricultural

68 biomass burning periods indicated that nighttime oxidation of biomass burning VOCs is dominated

69 by NO_3 (Decker et al., 2019). Hartikainen et al. (2018) reported high amounts of nitrogen-

70 containing organic compounds both in the gas and particle phase after dark aging of residential

71 wood combustion emissions. Kodros et al. (2020) reported significant and rapid OOA production

72 in laboratory experiments in which fresh biomass burning emissions were exposed to NO_3 and

73 suggested that dark oxidation may be an important process on regional scales. In the same study,

74 ambient measurements in an urban area suggested that the mixing of O_3 from the residual layer

75 down to the nocturnal boundary layer can enhance the formation of NO_3 and the nighttime

76 oxidation of biomass burning emissions. The mixing of ozone from the residual layer and the

77 importance to nightime chemistry was also suggested in studies on nightime oxidation of biogenic

78 VOCs (Brown et al., 2009; Brown et al., 2013). Despite this important finding, the degree to which

79 biomass burning plumes undergo night-time aging and produce significant amounts of SOA

80 remains poorly understood. Lacking consideration of such nocturnal chemistry in transport models

81 has been suggested as a possible source of the under prediction oxidized organic aerosol mass by

82 a factor of 3-5 (Fountoukis et al., 2016; Tsimpidi et al., 2014) during wintertime in polluted areas

83 with low photochemical activity.

84   Usually smog chamber studies use fresh biomass burning emissions generated in the

85 laboratory by a single source as a starting point of their experiments. The use of a dual chamber

86 system with starting point ambient air rich in biomass burning emissions but also primary and

87 secondary pollutants from other sources offers a bridge between traditional laboratory studies and

88 ambient observations. Such a system offers the capability of aging realistic biomass burning

89 emissions from multiple sources and fuels, diluted in the atmosphere and mixed with other

90 pollutants (e.g., NO_x from transportation). In this study, we take advantage of the high levels of

91 OA from residential biomass burning in Patras, Greece (the country's third-largest city), to

92 investigate the importance of night-time chemistry in the processing of biomass burning OA.

93 Biomass burning leads to concentrations of OA exceeding 50 μg m^{-3} in Patras in the early evening

94 (Florou et al., 2017). A dual atmospheric simulation chamber system is used to elucidate the
95 formation of SOA during winter periods in urban areas with high biomass burning organic aerosol
96 concentrations.
97
98 **2. Experimental Methods**
99 **2.1 Dual chamber system**
100 The dual chamber system developed by Kaltsonoudis et al. (2019) was used for
101 experiments in early 2020 in Patras, Greece during the PyroTRACH-PANACEA Wintertime 2020
102 experiment. The system consists of two 1.5 m^3 Teflon (PTFE) reactors attached to metallic frames.
103 Use of the second reactor as a reference (control chamber) allows the identification and potential
104 correction for any major experimental artifacts that could be due to the walls of the chamber and
105 the other complexities of this experimental system. The dual chamber system was deployed from
106 January 10 till February 15, 2020 in the city of Patras. The chambers along with the available
107 instrumentation were located indoors, in the campus of the University of Peloponnese,
108 approximately a few kilometers away from the center of the city (Figure S1). The windows of the
109 laboratory were kept open before and during the experiments, so the temperature of the dual
110 chamber system was in the 12-20°C range, while the outdoor temperature was on average 5 degrees
111 lower. The relative humidity (RH) in the chambers ranged from 35 to 45%.
112
113 **2.2 Experimental description**
114 Both chambers were flushed with ambient air before each experiment using a metal bellows
115 pump (Senior Aerospace, MB-602) for 1-2 h. This process is used to achieve higher sampling
116 efficiency and brings the system (chamber walls, tubing) close to equilibrium with ambient air
117 reducing losses of vapors to the sampling lines and walls of the chamber. Ambient air during
118 nighttime cold periods was introduced inside both chambers. In one of the chambers, (perturbed
119 chamber) ozone was added and upon reaction with the existing NO_x in the chamber formed NO_3
120 radicals. The second chamber (control chamber) was used as the reference in order to help us
121 understand the unperturbed evolution of the system inside the chamber. During all experiments
122 the chambers were under dark conditions. Ambient air was flushed through each of the chambers
123 with a flow of 80 L min^{-1}. More than 70% of the ambient PM was transferred to the chambers and
124 the concentrations of the measured VOCs were within 5% of their ambient values.

125   Using an automated valve switching between the two reactors, the particle and gas
126   concentrations in both chambers were measured. Data were collected 1.5 min after the switching
127   of the valve to avoid any memory effects related to the sampling lines. For the gas phase
128   measurements PTFE tubing (0.25 in) was used, while for the particle phase the tubing was copper
129   (0.25 in).

130   After filling the chambers with ambient air, the content of each chamber was characterized
131   for approximately one hour. The ozone added in the perturbed chamber after the characterization
132   period was in the range of 50-250 ppb. These values are higher than the 20 ppb measured during
133   the nighttime in Patras in this campaign, but some acceleration of the corresponding chemical
134   processes is necessary to reduce the effects of the walls and to limit the duration of the experiments
135   in the relatively small chambers used.

136   In selected experiments, approximately 40 ppb of d9-butanol was added in both chambers
137   to measure the OH concentration. Following Barnet et al. (2012), the OH concentration in the
138   chambers was estimated with the measured decay of the butanol concentration assuming a reaction
139   rate constant with OH of 3.4×10^{12} cm^3 molecule^{-1} s^{-1}.

140   An incoherent broad-band cavity-enhanced absorption spectroscopy (IBB-CEAS) was
141   used to measure the NO$_3$ radical concentration. Detailed information about the technique can be
142   found elsewhere (Venables et al., 2006; Ventrillard-Courtillot et al., 2010; Chen and Venables,
143   2011; Fouqueau et al., 2020). Briefly the light from a LED source centered on the 662 nm
144   absorption cross section of NO$_3$ radical is focused and introduced into a high-finesse optical cavity
145   composed of two high reflectivity (~99.98%) and 1 m curvature mirrors. The optical cavity has a
146   length of 0.61 m and allows up to 4.5 km (at 662 nm) optical path and a detection limit up to 3 ppt
147   (integration time of 10 seconds). Particle-free air is passed through the cavity at 2.5 L min^{-1}.
148   Spectra between 640 and 685 nm were recorded with an OceanOptics QE-65 Pro spectrometer. A
149   time resolution of one minute was selected for these experiments. Calibration with NO$_2$ (800 ppb
150   in dry nitrogen, Air Liquide) was performed daily in order to precisely determine the reflectivity
151   of the mirrors and estimate the optical path. The sample spectra were fitted against standard spectra
152   of gas species absorbing in the spectral region of the instrument: NO$_3$ radical (Orphal et al., 2003),
153   NO$_2$ (Vandaele et al., 1998) and H$_2$O (reference spectrum recorded with the instrument) using the
154   DOASIS software.

155   A quadrupole proton-transfer reaction mass spectrometer (PTR-MS, Ionicon Analytik) was

156   used to measure the concentration of VOCs including d9-butanol. We calculated the initial VOC

157   levels in the chambers using the concentrations of m/z 42 (acetonitrile), 69 (isoprene), 71 (MVK

158   & MACR), 73 (MEK), 79 (benzene), 93 (toluene) and 107 (xylene). We used the above m/z peaks,

159   because the PTR-MS was calibrated for those values. For the experiments that the PTR-MS was

160   not available we scaled the initial VOCs concentration using the black carbon (BC) levels. Using

161   a series of gas monitors the concentration of nitrogen oxides (NO and NO_2) and ozone (O_3) were

162   measured (Teledyne models: T201 and 400E respectively).

163   A TSI scanning mobility particle sizer (SMPS, classifier model 3080; DMA model 3081

164   CPC model 3775) was used for measuring the particle number distribution in the 15-700 nm range.

165   An Aerodyne high-resolution time-of-flight aerosol mass spectrometer (HR-ToF-AMS) was

166   measuring the composition and mass spectrum of OA. We did not use a dryer before the

167   instruments and the RH of the samples was recorded. For the analysis of the HR-ToF-AMS data

168   we used the AMS software toolkit (SQUIRREL v1.57I) and for the high-resolution data the Peak

169   Integration by Key Analysis (PIKA v1.16I) software. The elemental ratios were calculated using

170   the improved method of Canagaratna et al. (2015). The mass concentration and particle distribution

171   of BC were measured using a single-particle soot photometer (SP2, Droplet Measurement

172   Techniques).

173   The collection efficiency (CE) of the AMS was calculated applying the algorithm of

174   Kostenidou et al. (2007), comparing the SMPS volume distributions and the AMS mass

175   distributions. The CE ranged between 0.40-0.45 depending on the experiment. Using the same

176   algorithm, the density of the OA was calculated to be in the range of 1.25-1.4 g cm^{-3}.

177   Using the theta (θ) angle (Kostenidou et al., 2009) a comparison between the OA spectra

178   of the ambient and the chamber content after filling, we concluded that the OA composition

179   injected in the chambers was the same as in the ambient air. The theta angle between the two

180   chambers and the ambient OA spectra was always less than 4 degrees, suggesting excellent

181   agreement. Also, the OA mass spectra in the two chambers right after their filling was in very good

182   agreement (θ=3-4°), confirming that both chambers had the same OA composition initially. The θ

183   angle is a useful metric for the comparison of OA mass spectra, similar to the often used R^2. A θ

184   angle of two AMS spectra in the 0-5° range indicates an excellent match between the compared

185   spectra, which should be considered identical for all practical purposes (R^2 ranging from 1 to 0.99).

186   For a θ angle of 6-10° there is a good match (R^2 approximately 0.98-0.96), but there are some small

187   differences. A θ of 11-15° shows that the spectra are quite similar, but they are not the same (R^2:

188   0.95-0.92), while for a θ in the 16-30° range the spectra are coming from different sources, but

189   there are some similarities (R^2: 0.91-0.73). A θ angle higher than 30° suggests clearly different

190   AMS spectra. We use the θ angle in this study due to its ability to better represent relatively small

191   differences than the coefficient of determination.

192   Following the completion of each perturbation experiment, a wall-loss characterization

193   experiment was conducted to measure the size-dependent particle wall-loss rate constant inside

194   the two chambers (Wang et al., 2018). The particles were produced by the atomization (TSI, model

195   3076) of an aqueous solution of ammonium sulfate (5 g L^{-1}). The ammonium sulfate seeds after

196   the atomizer passed through a diffusion dryer and then were injected in the chambers without

197   passing through a neutralizer. Using an ionizing fan, the chamber walls were swept before the start

198   of each experiment to keep the particle loss rates low (Jorga et al., 2020).

199   The perturbation experiments started around 17:30-18:30 LT each evening (approximately

200   30 min after the sunset which during the campaign was from 17:00 to 18:00 LT), when the OA

201   concentration was elevated from local nocturnal biomass burning emissions in the area for heating.

202   The initial conditions in the experiments are summarized in Table 1. Thirteen experiments, eleven

203   involving perturbation and two blank experiments, in which no ozone was injected in either

204   chamber, were performed during January and February 2020 using ambient air from Patras.

205

3. Results

207   Our study was designed so that the experiments would start when biomass burning was the

208   major source of both organic aerosol and VOCs. In this section we first present in detail the results

209   of one typical experiment (Exp. 1) and then we summarize the results of the rest of the conducted

210   experiments. Exp. 1 started during an early evening period with moderate to high concentrations

211   of bbOA, VOCs, and NO_x (Table 1) and combined all the necessary elements to demonstrate the

212   behavior of the system studied.

213

3.1 Results of a typical perturbation experiment

215   The average PM_1 concentration in the chambers during the filling process of Exp. 1 was

216   approximately 50 µg m^{-3}. The concentration of OA during that period was 44 µg m^{-3} with 2.4 µg

217 m^{-3} of BC. The positive matrix factorization (PMF) analysis of the full campaign ambient data set

218 suggested that 70% of the OA at the time of filling originated from biomass burning (Kaltsonoudis

219 et al., 2021). Other OA sources included cooking OA or COA (15%), oxygenated OA or OOA

220 (10%) and hydrocarbon-like OA or HOA (5%). PMF was applied to the high resolution AMS

221 organic mass spectra (m/z up to 300) at 3 min resolution from the month long field campaign.

222 Solutions with one to seven factors were investigated. The best solution included 4 factors

223 corresponding to bbOA, OOA, COA and HOA. The time series of the four factors during the full

224 field campaign are shown in Figure S2. The detailed analysis of the field campaign, the

225 determination of the PMF factors as well as particle and gas measurements will be included in a

226 forthcoming publication.

227   The initial concentration of O_3 in the two chambers was 10 ppb, of NO 17 ppb and of NO_2

228 24 ppb, values within 5% of their ambient concentrations. The measured initial VOC levels were

229 approximately 150 $\mu g\ m^{-3}$ while the RH inside both chambers was approximately 45%. The rest

230 of the conditions are summarized in Table 1.

231   In Exp.1 NO_2 increased to 30 ppb in the perturbed chamber in approximately 30 min after

232 the ozone injection while at the same time NO levels dropped to close to zero. In the perturbed

233 chamber 2 hours after the injection the mixing ratio of NO_2 was 18 ppb and of ozone 220 ppb. In

234 the control chamber the concentrations of the above mentioned gases remained within 10% of their

235 initial levels. Due to the time needed for mixing and the rapid reaction of NO and O_3 it is difficult

236 to measure accurately the injected O_3 concentration. A zeroth order estimate can be made assuming

237 that the injected amount of ozone is equal to the final (equilibrated) amount of ozone in the

238 perturbed chamber plus the reacted NO_x (Table S1). Based on this zeroth order estimate, the

239 injected ozone in Exp. 1 was approximately 240 ppb.

240   Following the injection of ozone in the perturbed chamber (t=0 h) there was a rapid increase

241 of OA (Figure 1). Approximately 33 $\mu g\ m^{-3}$ of SOA was produced in 2.5 hours (70% increase from

242 the initial injected OA levels). In just one hour after the injection of ozone, the OA concentration

243 increased by approximately 25 $\mu g\ m^{-3}$. This high rate secondary OA production rate of

244 approximately 25 $\mu g\ m^{-3}\ h^{-1}$is at least partially due to the high ozone levels used in these

245 experiments to accelerate the corresponding chemistry and reduce the problems caused by losses

246 of both particles and vapors to the walls of the chamber. Although this formation rate is true under

247 high ozone levels, the absolute increase in the OA concentration indicates the strong potential of

the ambient air in an urban area with strong biomass burning emissions to form SOA even under dark conditions. The change of OA in the control chamber after the particle wall-loss corrections was less than 7% at all times. This strongly indicates that the OA changes in the perturbation chamber were not due to experimental artifacts.

The sulfate concentration remained practically the same (within 10%) in both the perturbed and the control chambers after accounting for particle wall-losses. The initial nitrate in the perturbed chamber was 1 μg m^{-3} more than in the control. This small difference can be an artifact of the sampling system in this specific experiment. Production of approximately 6 μg m^{-3} of aerosol nitrate was observed in the perturbed chamber with the majority of this increase in the form of organic nitrate. Using the method described in Farmer et al. (2010) using the NO^+/NO_2^+ ratio from the AMS, we estimate that close to 60% of the formed secondary aerosol nitrate in the perturbed chamber was organic nitrate. Details of the organic nitrate estimation approach can be found in the Supplemental Information of the paper. Taking into account the organic nitrate, there was a 77% increase of the OA compared to the initial concentration.

An increase of the ammonium concentration by close to 1 μg m^{-3} was observed in the perturbed chamber (a 90% increase of ammonium compared to its levels before the injection of ozone) while in the control chamber its concentration remained within 8% of the initial value. Most of this increase was due to the formation of ammonium nitrate. Approximately 40% of the total nitrate formed was inorganic nitrate, which requires approximately 1 μg m^{-3} of ammonium to be neutralized. So the increase in ammonium is consistent with the increase in inorganic assuming that ammonium nitrate was formed.

3.2 Organic aerosol spectra

Figure 2 represents the OA mass spectra in the two chambers at the start and end of Exp.1. The comparison of the OA mass spectra in the perturbed chamber at the beginning (after the air injection) and at the end (2.5 hours after the ozone injection) of Exp. 1 indicates that there was an increase in the fractional signal of m/z: 28 (CO^+), 29 (CHO^+), 30 (CH_2O^+), 43 ($C_2H_3O^+$), and 44 (CO_2^+). The highest decrease was observed in 55 ($C_4H_7^+$), 57 ($C_4H_9^+$), 60 ($C_2H_4O_2^+$), 69 ($C_5H_9^+$), 91 ($C_7H_7^+$) and 95 ($C_7H_{11}^+$). The theta angle between the spectra was 19 degrees, indicating significant change. The initial and final spectra in the control chamber had a θ angle of 8 degrees, with changes in m/z 28, 44, 57 and 60.

279   The O:C ratio in the control chamber remained practically constant during Exp. 1, with a
280   value close to 0.4 (Figure 3). This suggests that there was relatively low chemical activity in this
281   chamber. This is consistent with the small change in the OA mass spectrum. This activity is could
282   be due to the existing O_3 and any produced NO_3 in the control chamber. On the contrary in the
283   perturbed chamber after the injection of ozone the O:C ratio increased rapidly reaching 0.52 after
284   30 min. At the end of the experiment, the O:C ratio in the perturbed chamber reached a value of
285   0.61, similar to the measured ambient value around 3:00 LT at night.

286   To calculate the mass spectrum of the produced OA in the perturbed chamber, we used a
287   simple mass balance approach. Details about this method can be found in Jorga et al. (2020).
288   Concisely, assuming that the main processes in the chamber are losses of particles to the chamber
289   walls and SOA formation, we estimate the initial (before the injection of ozone) and produced OA
290   mass spectra. Using the size-dependent particle loss rate constant measured at the end of each
291   experiment, the concentration of the pre-existing OA as a function of time can be calculated. The
292   pre-existing OA concentration in the perturbation chamber decreased from approximately 30 to 12
293    $\mu g\ m^{-3}$ during Exp. 1 (Figure 4). Additional information about the particle loss correction approach
294   together with the size dependence of the particle loss rate constants for Exp. 1 (Figure S3) can be
295   found in the SI. The produced SOA that remains suspended in the chamber is then the difference
296   between the total measured and the pre-existing or "initial" OA (Figure 4). The maximum
297   concentration of the produced SOA was 23 $\mu g\ m^{-3}$, but it was gradually reduced to 15 $\mu g\ m^{-3}$ due
298   to the particle losses to the walls. With the concentrations of the pre-existing OA and the produced
299   SOA both suspended in the chamber (these are the actual concentrations not corrected for wall
300   losses) the AMS spectra that correspond to the sum of the two, the spectrum of the produced SOA
301   can be estimated. Figure 5 shows the resulting spectra for the produced SOA both for Exp. 1 and
302   the average SOA spectra for all the experiments. The similarity of the spectra supports our choice
303   of Exp. 1 as representative of the rest.

304   Our estimation of the produced SOA levels is based on the mass balance approach of Jorga
305   et al. (2020) and not on the yields and concentration reduction of individual VOCs. Given the
306   uncertainties in the concentrations and the yields of the various VOCs and IVOCs in this complex
307   system this is a more accurate estimate. We assume that the main process responsible for the
308   reduction of the initial OA is loss of particles to the walls and that the loss of particle mass by
309   evaporation and then loss of the vapors to the walls is negligible. The accuracy of this assumption

can be confirmed by the change of the OA in the reference chamber (Figure 1a). The small change of the particle wall loss-corrected OA concentration (less than 7%) supports our assumption. If evaporation and vapor wall loss were important processes the corresponding concentration in the reference chamber would be decreasing significantly. This is one of the advantages of our approach using ambient air. The evaporation of the bbOA after its emission has already taken place in the atmosphere. Therefore, the SOA production that we measure does account for the SVOCs that have moved to the gas-phase as the bbOA gets diluted in the atmosphere. The changes in the reference chamber illustrate well the changes that continue to happen in the system without our acceleration of the chemistry.

The produced OA mass spectra from the perturbed chamber were compared with the produced OA factor from the dark aging of biomass burning emissions in the laboratory (Kodros et al., 2020). Although the present study deals with emissions from multiple biomass burning sources and fuels in a complex air mixture and varying conditions compared to the laboratory work (that used specific biomass burning emissions under idealized conditions) a comparison can provide us with information about the consistency of the two studies. Kodros et al. (2020) performed chamber experiments in which they exposed residential biomass burning emissions from a residential wood stove to NO_2 and O_3 under different RH conditions. Here, we compare the produced OA from a medium RH (approximately 45%) experiment with those of the ambient perturbation experiments that had similar RH. The θ angle between the produced OA from perturbation Exp.1 and the one from the laboratory chamber experiment was 11 degrees, indicating a considerable degree of similarity (Figure 6). The comparison of our results with the work of Kodros et al. (2020) can also be viewed as an independent test of the validity of our assumption that most of the SOA formed in our experiments was indeed due to biomass burning. This previous study used only biomass burning emissions therefore there is no doubt that their results represent bbSOA. The good comparison of the produced SOA spectra in the two studies both strengthens our argument that we mainly observe bbSOA formation and also strengthens the argument of Kodros et al. (2020) that their laboratory results are a reasonable representation of realistic atmospheric processing of biomass burning emissions.

The produced OA was also compared with the ambient oxygenated organic aerosol (OOA) factor identified from the PMF analysis of the ambient data. The θ angle between the ambient OOA in Patras from winter 2020 and the produced OA from Exp. 1 was 10 degrees. Similarities

341 were also observed in the produced OA and OOA from cities around the world during winter
342 periods. For Exp. 1 the θ angle was in the range of 9-18 degrees (Table S2) when compared with
343 OOA factors from Fresno, US (Ge et al., 2012), Barcelona, Spain (Mohr et al., 2012), Paris, France
344 (Crippa et al., 2013), Bologna, Italy (Gilardoni et al., 2016), Athens, Greece (Florou et al., 2017)
345 and Xi'an/Beijing, China (Elser et al., 2016). The contribution of biomass burning to the measured
346 OA in the above field studies ranged from 16% (Fresno, California) up to 70% (Patras and Athens,
347 Greece). The OOA as viewed by the PMF analysis of the AMS spectra has most of the time little
348 information about its source. Therefore, this similarity just strengthens our argument that the SOA
349 produced in our experiments was rather realistic. We further compared the AMS spectrum of the
350 SOA produced in this study with the spectra of the SOA produced during daytime oxidation of
351 biomass burning emissions in the laboratory (Kodros et al., 2020). There are notable differences
352 in the two spectra, with theta angles approaching 30 degrees.

353

354 **3.3 Results of other experiments**

355 The rapid OA production observed during Exp. 1 was also observed in all the other
356 experiments, with approximately 75% of the produced OA formed in the first hour after the ozone
357 injection. The injected ozone levels in the other experiments, excluding Exp. 1 ranged from 65 to
358 220 ppb. Figure 7 shows the produced OA (including organic nitrates) in all the perturbation
359 experiments. In all experiments, the majority of secondary aerosol nitrate was organic,
360 representing 55-85% of the total produced nitrate. Taking into account the organic nitrates, the
361 initial SOA formation rate in the perturbed chamber in the conducted experiments was on average
362 10 μg m^{-3} h^{-1}, ranging from 1 to 30 μg m^{-3} h^{-1}.

363 An increase in the O:C in the perturbed chamber was observed in all experiments with an
364 average increase from the initial O:C of 45% At the same time, the O:C in the control chamber
365 remained within 6% of the initial value. Table S3 summarizes the OA enhancement and the initial
366 and final O:C in the perturbed chamber in the conducted experiments.

367 The mass spectra of the produced OA in the perturbed chamber were similar to that of
368 Exp.1 with the major m/z values being 28, 29, 43, 44, 55 and 69 (Figure 5). The θ angle between
369 the different produced OA spectra in the perturbed experiments were less than 14 degrees,
370 suggesting similarities between the produced OA from the different perturbation experiments. The
371 θ angle between the produced OA mass spectra in the perturbed chamber and the one from Kodros

372 et al. (2020) was in the range of 9-16 degrees, suggesting similarity of the results of the two studies,
373 even if one relied on a single fuel burned in a single stove and the other in a mixture of emissions
374 from thousands of fireplaces and heating stoves. Another possible explanation of the difference
375 between the two studies is the presence of non-biomass burning emissions in the urban ambient
376 air that could contribute to the SOA formation.

377

378 **3.4 NO_3 and OH radical levels**

379 Based on the decay of d9-butanol after the injection of ozone, the OH concentration was
380 in the range of $0.2-0.4\times10^6$ molecules cm^{-3} in the perturbation chamber suggesting that the addition
381 of ozone and reactions with organic vapors were not producing significant OH levels. Given the
382 sunlight in Greece even during the winter, these levels correspond to less than 10% of the daytime
383 OH in the area during that wintertime period. Despite the relatively low OH in the perturbation
384 chamber, its corresponding reactions with the various VOCs present do contribute to the observed
385 chemical changes. The characteristic reaction times with the OH of some of the VOCs present
386 (toluene, xylenes, isoprene, monoterpenes and phenol) that could contribute to SOA formation
387 ranged from approximately 9 to 160 hours suggesting that these reactions had a small contribution
388 to the rapid SOA formation observed during the first 30 min of a typical experiment (Figure 1).
389 The corresponding OH concentrations in the control chamber were practically zero and below the
390 detection levels of the d9-butanol approach. Measurements of the OH levels were only possible
391 when the PTR-MS was available (Exps 9-11), but the results were pretty consistent. Some OH
392 production is also expected in the ambient atmosphere as the ozone mixes in the nighttime
393 boundary layer from aloft, so these reactions are also taking place, albeit slowly, in the ambient
394 atmosphere too.

395 Nitrate radical concentrations above the detection level of a few ppt were only measured
396 in the perturbed chamber after the ozone injection. Overall NO_3 radical measurements were not
397 available during four out of the eleven experiments, but in two experiments (Exps. 3 and 10) the
398 NO_3 concentrations were below the instrument's detection limit. The maximum NO_3 radical
399 concentrations in the perturbed chamber ranged from 3 to 25 ppt with the highest observed during
400 Exp. 8 (Table S3). In this experiment before the ozone injection the NO_3 levels in both chambers
401 were below the detection limit of the instrument, while after the injection (t=0 h) the concentration
402 of NO_3 started to increase (Figure S4). In Exp. 8 there were 44 ppb of NO_x initially and 150 ppb

403   of O_3 were injected. Approximately 15 µg m^{-3} of OA was formed in 2.5 h after the perturbation,

404   with close to 2 µg m^{-3} of the OA formed being organic nitrate. The O:C reached a value of 0.6 at

405   the end of this experiment.

406   The measured NO_3 concentrations along with the low concentrations of OH in the

407   perturbed chamber suggests that the reactions of VOCs with NO_3 radicals and potentially ozone

408   were the major source of SOA production.

409

410   **3.5 Factors affecting the SOA production**

411   The highest produced SOA was observed, as expected, in experiments that had high initial

412   OA and VOC levels. Experiments 1, 4 and 6 had the highest measured inital VOC levels among

413   the conducted experiments, close to 150 µg m^{-3} (Table 1). Although, only a fraction of the VOCs

414   present in the atmosphere were measured by the PTR-MS in this work, these measurements

415   provide an indication of the SOA formation potential of the corresponding air masses. We could

416   not identify a strong link between the small variations in the speciation of the initial VOCs and the

417   SOA or the organic nitrate formed. This is probably due to the fact that we quantified only a small

418   fraction of the VOCs and IVOCs that serve as SOA precursors in the system.

419   The absolute concentration of SOA formed was also affected by the levels of NO present.

420   Experiments with low initial NO, less than 5 ppb, (Experiments 2, 3, 5 ,9 and 11) had the lowest

421   SOA production. The lowest NO_3 radical concentrations were also observed in those experiments.

422   This is due to the low NO_x availability in the atmosphere during these experiments. These low

423   NO_x levels result in low NO_3 levels in the perturbed chamber and therefore together with the

424   relatively low VOC levels, during the same periods, lead to low SOA production. Figure 8 shows

425   the correlation between the concentration of NO_3 radicals and the produced organic nitrate levels

426   in the perturbed chamber. The good correlation (R^2=0.79) supports the strong link between the

427   NO_3 chemistry occurring in the perturbed chamber and the corresponding SOA production. This

428   correlation is driven by the results of two experiments with high NO_3 radical levels and high

429   organic nitrate concentrations in the particulate phase. This suggests that the oxidants levels

430   (mainly NO_3) produced after reactions of ozone with the pre-existing NO_x are affecting

431   significantly the levels of SOA formed under these conditions. We estimated an R^2=0.66 between

432   the formed SOA and the levels of NO_3 in the perturbed chamber (Figure S5).

433

4. Conclusions

In this work, we studied the nighttime aging of urban wintertime air, strongly influenced by biomass burning emissions in Patras, Greece. Using a dual chamber system and ambient air as a starting point, we injected additional ozone in only one chamber to accelerate nitrate radical production via reactions with the pre-existing NO_x. The other chamber was used as a reference mainly as a safeguard against potential experimental artifacts. The novelty of this experimental approach is that it allowed the quantification of the nighttime chemical transformations of realistic biomass burning emissions from thousands of sources and multiple fuels after they had been diluted and mixed with ambient air. Our experiments took place during periods in which biomass burning was responsible for 70% on average of the ambient OA and therefore the biomass burning emissions were the dominant source of VOCs and IVOCs.

After the addition of ozone, rapid SOA formation was observed in the perturbed chamber with the additional OA formed reaching up to 35 μg m^{-3}. The SOA formed increased the pre-existing OA by 20-70%. Most of the secondary nitrate formed was organic nitrate, in some cases reaching up to 85% of the total aerosol nitrate. On average 10% of the total OA formed was organic nitrate. The organic aerosol formation was rapid, with 75% of the produced OA formed in the first hour after the ozone injection. The organic aerosol content in the control chamber remained within 10% of the initial levels, suggesting limited chemical oxidation without the addition of ozone in these timescales. These results strongly suggest that significant secondary OA can be formed even during the nighttime of winter periods through the chemical processing of biomass burning emissions.

The O:C of organic aerosol increased rapidly in the perturbed chamber following the ozone injection. In 2-3 h of reactions a 40-50% increase of the O:C was observed while the OA O:C in the control chamber remained within approximately 5% of the initial value. The produced OA mass spectra showed similarities with the produced OA factor from dark aging biomass burning experiments under laboratory conditions, pointing towards the important role of biomass burning emissions in the OA formed in a winter urban environment. Furthermore, the produced SOA mass spectra were quite similar to those of ambient oxygenated OA factors found in urban areas during winter periods in which the fresh bbOA contributed 15-70% of the OA.

Nitrate radicals were observed only in the perturbed chamber and only after the ozone injection. Their levels reached up to 25 ppt. The low and steady levels of hydroxyl radical in the

465 perturbed chamber along with the high characteristic reactions times of the measured VOCs with

466 the OH compared to the duration of the experiments, indicates that reaction with nitrate radicals

467 and ozone were responsible for the SOA formation and the change in the OA composition.

468

469 *Author Contribution*: S.D.J., K.F., C.K., J.K.K. and C.V. conducted the experiments, collected and

470 analyzed the data. S.N.P and A.N. conceived and directed the study. M.C., A.F. and B.P.-V.

471 provided the IBB-CEAS. S.D.J. and S.N.P. wrote the manuscript with inputs from all co-authors.

472

473 *Data availability*: Data related to this article are available upon request to the corresponding author.

474 The data will be available in the EUROCHAMP-2020 website.

475

476 *Competing interests*: The authors declare that they have no conflict of interest.

477

484

485 **References**

486 Ahern, A. T., Robinson, E. S., Tkacik, D. S., Saleh, R., Hatch, L. E., Barsanti, K. C., Stockwell,

487   C. E., Yokelson, R. J., Presto, A. A., Robinson, A. L., Sullivan, R. C. and Donahue, N. M.:

488   Production of secondary organic aerosol during aging of biomass burning smoke from

489   fresh fuels and its relationship to VOC precursors, J. Geophys. Res., 124, 3583–3606, 2019.

490 Akagi, S. K., Yokelson, R. J., Wiedinmyer, C., Alvarado, M. J., Reid, J. S., Karl, T., Crounse, J.

491   D. and Wennberg, P. O.: Emission factors for open and domestic biomass burning for use

492   in atmospheric models, Atmos. Chem. Phys., 11, 4039–4072, 2011.

493 Akherati, A., He, Y., Coggon, M. M., Koss, A. R., Hodshire, A. L., Sekimoto, K., Warneke, C.,

494   De Gouw, J., Yee, L., Seinfeld, J. H., Onasch, T. B., Herndon, S. C., Knighton, W. B.,

495   Cappa, C. D., Kleeman, M. J., Lim, C. Y., Kroll, J. H., Pierce, J. R. and Jathar, S. H.:

Oxygenated aromatic compounds are important precursors of secondary organic aerosol in biomass-burning emissions, Environ. Sci. Technol., 54, 8568–8579, 2020.

Alfarra, M. R., Prevot, A. S. H., Szidat, S., Sandradewi, J., Weimer, S., Lanz, V. A., Schreiber, D., Mohr, M. and Baltensperger, U.: Identification of the mass spectral signature of organic aerosols from wood burning emissions, Environ. Sci. Technol., 41, 5770–5777, 2007.

Andreae, M. O. and Merlet, P.: Emission of trace gases and aerosols from biomass burning, Global Biogeochem. Cycles, 15, 955–966, 2001.

Bond, T. C., Streets, D. G., Yarber, K. F., Nelson, S. M., Woo, J. H. and Klimont, Z.: A technology-based global inventory of black and organic carbon emissions from combustion, J. Geophys. Res., 109, D14203, doi:10.1029/2003JD003697, 2004.

Bougiatioti, A., Stavroulas, I., Kostenidou, E., Zarmpas, P., Theodosi, C., Kouvarakis, G., Canonaco, F., Prévôt, A. S. H., Nenes, A., Pandis, S. N. and Mihalopoulos, N.: Processing of biomass-burning aerosol in the eastern Mediterranean during summertime, Atmos. Chem. Phys., 14, 4793–4807, 2014.

Boy, J., Rollenbeck, R., Valarezo, C. and Wilcke, W.: Amazonian biomass burning-derived acid and nutrient deposition in the north Andean montane forest of Ecuador, Global Biogeochem. Cycles, 22, GB4011, 2008.

Brown, S. S., deGouw, J. A., Warneke, C., Ryerson, T. B., Dubé, W. P., Atlas, E., Weber, R. J., Peltier, R. E., Neuman, J. A., Roberts, J. M., Swanson, A., Flocke, F., McKeen, S. A., Brioude, J., Sommariva, R., Trainer, M., Fehsenfeld, F. C., and Ravishankara, A. R.: Nocturnal isoprene oxidation over the Northeast United States in summer and its impact on reactive nitrogen partitioning and secondary organic aerosol, Atmos. Chem. Phys., 9, 3027–3042, 2009

Brown, S. S., Dubé, W. P., Bahreini, R., Middlebrook, A. M., Brock, C. A., Warneke, C., de Gouw, J. A., Washenfelder, R. A., Atlas, E., Peischl, J., Ryerson, T. B., Holloway, J. S., Schwarz, J. P., Spackman, R., Trainer, M., Parrish, D. D., Fehshenfeld, F. C., and Ravishankara, A. R.: Biogenic VOC oxidation and organic aerosol formation in an urban nocturnal boundary layer: aircraft vertical profiles in Houston, TX, Atmos. Chem. Phys., 13, 11317–11337, 2013.

525   Bruns, E. A., El Haddad, I., Slowik, J. G., Kilic, D., Klein, F., Baltensperger, U. and Prévôt, A. S.

526   H.: Identification of significant precursor gases of secondary organic aerosols from

527   residential wood combustion, Sci. Rep., 6, 27881, 2016.

528   Canagaratna, M. R., Jimenez, J. L., Kroll, J. H., Chen, Q., Kessler, S. H., Massoli, P., Hildebrandt

529   Ruiz, L., Fortner, E., Williams, L. R., Wilson, K. R., Surratt, J. D., Donahue, N. M., Jayne,

530   J. T. and Worsnop, D. R.: Elemental ratio measurements of organic compounds using

531   aerosol mass spectrometry: characterization, improved calibration, and implications,

532   Atmos. Chem. Phys., 15, 253–272, 2015.

533   Capes, G., Johnson, B., McFiggans, G., Williams, P. I., Haywood, J. and Coe, H.: Aging of

534   biomass burning aerosols over West Africa: Aircraft measurements of chemical

535   composition, microphysical properties, and emission ratios, J. Geophys. Res., 113, 1–13,

536   2008.

537   Crippa, M., DeCarlo, P. F., Slowik, J. G., Mohr, C., Heringa, M. F., Chirico, R., Poulain, L.,

538   Freutel, F., Sciare, J., Cozic, J., Di Marco, C. F., Elsasser, M., Nicolas, J. B., Marchand,

539   N., Abidi, E., Wiedensohler, A., Drewnick, F., Schneider, J., Borrmann, S., Nemitz, E.,

540   Zimmermann, R., Jaffrezo, J.-L., Prévôt, A. S. H. and Baltensperger, U.: Wintertime

541   aerosol chemical composition and source apportionment of the organic fraction in the

542   metropolitan area of Paris, Atmos. Chem. Phys., 13, 961–981, 2013.

543   Decker, Z. C. J., Zarzana, K. J., Coggon, M., Min, K. E., Pollack, I., Ryerson, T. B., Peischl, J.,

544   Edwards, P., Dubé, W. P., Markovic, M. Z., Roberts, J. M., Veres, P. R., Graus, M.,

545   Warneke, C., De Gouw, J., Hatch, L. E., Barsanti, K. C. and Brown, S. S.: Nighttime

546   chemical transformation in biomass burning plumes: A box model analysis initialized with

547   aircraft observations, Environ. Sci. Technol., 53, 2529–2538, 2019.

548   Elser, M., Huang, R.-J., Wolf, R., Slowik, J. G., Wang, Q., Canonaco, F., Li, G., Bozzetti, C.,

549   Daellenbach, K. R., Huang, Y., Zhang, R., Li, Z., Cao, J., Baltensperger, U., El-Haddad, I.

550   and Prévôt, A. S. H.: New insights into $PM_{2.5}$ chemical composition and sources in two

551   major cities in China during extreme haze events using aerosol mass spectrometry, Atmos.

552   Chem. Phys., 16, 3207–3225, 2016.

553   Farmer, D. K., Matsunaga, A., Docherty, K. S., Surratt, J. D., Seinfeld, J. H., Ziemann, P. J. and

554   Jimenez, J. L.: Response of an aerosol mass spectrometer to organonitrates and

555   organosulfates and implications for atmospheric chemistry, Proc. Natl. Acad. Sci.., 107,
556   6670–6675, 2010.

557 Favez, O., El Haddad, I., Piot, C., Boréave, A., Abidi, E., Marchand, N., Jaffrezo, J.-L., Besombes,
558   J.-L., Personnaz, M.-B., Sciare, J., Wortham, H., George, C. and D'Anna, B.: Inter-
559   comparison of source apportionment models for the estimation of wood burning aerosols
560   during wintertime in an Alpine city (Grenoble, France), Atmos. Chem. Phys., 10, 5295–
561   5314, 2010.

562 Florou, K., Papanastasiou, D. K., Louvaris, E., Kaltsonoudis, C., Patoulias, D., Pikridas, M.,
563   Gkatzelis, G. I., Pandis, S. N. and Mihalopoulos, N.: The contribution of wood burning and
564   other pollution sources to wintertime organic aerosol levels in two Greek cities, Atmos.
565   Chem. Phys., 17, 3145–3163, 2017.

566 Ford, B., Val Martin, M., Zelasky, S. E., Fischer, E. V., Anenberg, S. C., Heald, C. L. and Pierce,
567   J. R.: Future fire impacts on smoke concentrations, visibility, and health in the contiguous
568   United States, GeoHealth, 2, 229–247, 2018.

569 Fouqueau, A., Cirtog, M., Cazaunau, M., Pangui, E., Zapf, P., Siour, G., Landsheere, X., Méjean,
570   G., Romanini, D., and Picquet-Varrault, B.: Implementation of an incoherent broadband
571   cavity-enhanced absorption spectroscopy technique in an atmospheric simulation chamber
572   for in situ NO3 monitoring: characterization and validation for kinetic studies, Atmos.
573   Meas. Tech., 13, 6311–6323, 2020.

574 Fountoukis, C., Megaritis, A. G., Skyllakou, K., Charalampidis, P. E., Denier van der Gon, H. A.
575   C., Crippa, M., Prévôt, A. S. H., Fachinger, F., Wiedensohler, A., Pilinis, C. and Pandis, S.
576   N.: Simulating the formation of carbonaceous aerosol in a European Megacity (Paris)
577   during the MEGAPOLI summer and winter campaigns, Atmos. Chem. Phys., 16, 3727–
578   3741, 2016.

579 Fuller, G. W., Tremper, A. H., Baker, T. D., Yttri, K. E. and Butterfield, D.: Contribution of wood
580   burning to PM10 in London, Atmos. Environ., 87, 87–94, 2014.

581 Ge, X., Setyan, A., Sun, Y. and Zhang, Q.: Primary and secondary organic aerosols in Fresno,
582   California during wintertime: Results from high resolution aerosol mass spectrometry, J.
583   Geophys. Res., 117, D19301, doi:10.1029/2012JD018026, 2012.

584 Gilardoni, S., Massoli, P., Paglione, M., Giulianelli, L., Carbone, C., Rinaldi, M., Decesari, S.,
585   Sandrini, S., Costabile, F., Gobbi, G. P., Pietrogrande, M. C., Visentin, M., Scotto, F.,

Fuzzi, S. and Facchini, M. C.: Direct observation of aqueous secondary organic aerosol from biomass-burning emissions, Proc. Natl. Acad. Sci., 113, 10013–10018, 2016.

Hartikainen, A., Yli-Pirilä, P., Tiitta, P., Leskinen, A., Kortelainen, M., Orasche, J., Schnelle-Kreis, J., Lehtinen, K. E. J., Zimmermann, R., Jokiniemi, J. and Sippula, O.: Volatile organic compounds from logwood combustion: Emissions and transformation under dark and photochemical aging conditions in a smog chamber, Environ. Sci. Technol., 52, 4979–4988, 2018.

Hennigan, C. J., Miracolo, M. A., Engelhart, G. J., May, A. A., Presto, A. A., Lee, T., Sullivan, A. P., McMeeking, G. R., Coe, H., Wold, C. E., Hao, W.-M., Gilman, J. B., Kuster, W. C., de Gouw, J., Schichtel, B. A., Collett, J. L., Kreidenweis, S. M. and Robinson, A. L.: Chemical and physical transformations of organic aerosol from the photo-oxidation of open biomass burning emissions in an environmental chamber, Atmos. Chem. Phys., 11, 7669–7686, 2011.

Jolleys, M. D., Coe, H., McFiggans, G., Taylor, J. W., O'Shea, S. J., Le Breton, M., Bauguitte, S. J.-B., Moller, S., Di Carlo, P., Aruffo, E., Palmer, P. I., Lee, J. D., Percival, C. J. and Gallagher, M. W.: Properties and evolution of biomass burning organic aerosol from Canadian boreal forest fires, Atmos. Chem. Phys., 15, 3077–3095, 2015.

Jorga, S. D., Kaltsonoudis, C., Liangou, A. and Pandis, S. N.: Measurement of formation rates of secondary aerosol in the ambient urban atmosphere using a dual smog chamber system, Environ. Sci. Technol., 54, 1336–1343, 2020.

Kaltsonoudis, C., Jorga, S. D., Louvaris, E., Florou, K. and Pandis, S. N.: A portable dual-smog-chamber system for atmospheric aerosol field studies, Atmos. Meas. Tech., 12, 2733–2743, 2019.

Kaltsonoudis, C., Florou, K., Kodros, J., Jorga, S., Vasilakopoulou, C., Baliaka, C., Aktypis, A., Nenes, A. And Pandis, S. N.: Contribution of residential wood burning to wintertime air pollution in an urban area, European Geophysical Union General Assembly 2021, EGU21-10670, doi: 10.5194/egusphere-egu21-10670.

Kodros, J. K., Papanastasiou, D. K., Paglione, M., Masiol, M., Squizzato, S., Florou, K., Skyllakou, K., Kaltsonoudis, C., Nenes, A. and Pandis, S. N.: Rapid dark aging of biomass burning as an overlooked source of oxidized organic aerosol, Proc. Natl. Acad. Sci., 52, 33028-33033, 2020.

617 Kostenidou, E., Pathak, R. K. and Pandis, S. N.: An algorithm for the calculation of secondary

618   organic aerosol density combining AMS and SMPS data, Aerosol Sci. Technol., 41, 1002–

619   1010, 2007.

620 Kostenidou, E., Lee, B. H., Engelhart, G. J., Pierce, J. R. and Pandis, S. N.: Mass spectra

621   deconvolution of low, medium, and high volatility biogenic secondary organic aerosol,

622   Environ. Sci. Technol., 43, 4884–4889, 2009.

623 Mohr, C., DeCarlo, P. F., Heringa, M. F., Chirico, R., Slowik, J. G., Richter, R., Reche, C.,

624   Alastuey, A., Querol, X., Seco, R., Peñuelas, J., Jiḿenez, J. L., Crippa, M., Zimmermann,

625   R., Baltensperger, U. and Prév̂ot, A. S. H.: Identification and quantification of organic

626   aerosol from cooking and other sources in Barcelona using aerosol mass spectrometer data,

627   Atmos. Chem. Phys., 12, 1649–1665, 2012.

628 O'Dell, K., Ford, B., Fischer, E. V. and Pierce, J. R.: Contribution of Wildland-Fire Smoke to US

629   PM 2.5 and Its Influence on Recent Trends, Environ. Sci. Technol., 53, 1797–1804, 2019.

630 Orphal, J., Fellows, C. E., and Flaud, P.-M.: The visible absorption spectrum of NO_3 measured by

631   high-resolution Fourier transform spectroscopy, J. Geophys. Res., 108, 4077,

632   doi:10.1029/2002JD002489, 2003.

633 Ortega, A. M., Day, D. A., Cubison, M. J., Brune, W. H., Bon, D., De Gouw, J. A. and Jimenez,

634   J. L.: Secondary organic aerosol formation and primary organic aerosol oxidation from

635   biomass-burning smoke in a flow reactor during FLAME-3, Atmos. Chem. Phys., 13,

636   11551–11571, 2013.

637 Robinson, A. L., Subramanian, R., Donahue, N. M., Bernardo-Bricker, A. and Rogge, W. F.:

638   Source apportionment of molecular markers and organic aerosol. 2. Biomass smoke,

639   Environ. Sci. Technol., 40, 7811–7819, 2006.

640 Sundarambal, P., Balasubramanian, R., Tkalich, P. and He, J.: Impact of biomass burning on

641   Ocean water quality in Southeast Asia through atmospheric deposition: Field observations,

642   Atmos. Chem. Phys., 10, 11323–11336, 2010.

643 Tkacik, D. S., Robinson, E. S., Ahern, A., Saleh, R., Stockwell, C., Veres, P., Simpson, I. J.,

644   Meinardi, S., Blake, D. R., Yokelson, R. J., Presto, A. A., Sullivan, R. C., Donahue, N. M.

645   and Robinson, A. L.: A dual-chamber method for quantifying the effects of atmospheric

646   perturbations on secondary organic aerosol formation from biomass burning emissions, J.

647   Geophys. Res., 122, 6043–6058, 2017.

648 Tsimpidi, A. P., Karydis, V. A., Pozzer, A., Pandis, S. N. and Lelieveld, J.: ORACLE (v1.0):
649   module to simulate the organic aerosol composition and evolution in the atmosphere,
650   Geosci. Model Dev., 7, 3153–3172, 2014.

651 Vakkari, V., Beukes, J. P., Dal Maso, M., Aurela, M., Josipovic, M. and van Zyl, P. G.: Major
652   secondary aerosol formation in southern African open biomass burning plumes, Nat.
653   Geosci., 11, 580–583, 2018.

654 Vandaele, A. C., Hermans, C., Simon, P. C., Carleer, M., Colin, R., Fally, S., Mérienne, M. F.,
655   Jenouvrier, A., and Coquart, B.: Measurements of the NO_2 absorption cross-section from
656   42 000 cm^{-1} to 10 000 cm^{-1} (238–1000 nm) at 220K and 294 K., J. Quant. Spectrosc. Radiat.
657   Transf., 59, 171–184, 1998.

658 Wang, N., Jorga, S. D., Pierce, J. R., Donahue, N. M. and Pandis, S. N.: Particle wall-loss
659   correction methods in smog chamber experiments, Atmos. Meas. Tech., 11, 6577–6588,
660   2018.

661 Watson, J. G.: Visibility: Science and regulation, J. Air Waste Manag. Assoc., 52, 628–713, 2002.

662 Yu, J., Cocker, D. R., Griffin, R. J., Flagan, R. C. and Seinfeld, J. H.: Gas-phase ozone oxidation
663   of monoterpenes: Gaseous and particulate products, J. Atmos. Chem., 34, 207–258, 1999.

664 Zhao, D. F., Kaminski, M., Schlag, P., Fuchs, H., Acir, I.-H., Bohn, B., Häseler, R., Kiendler-
665   Scharr, A., Rohrer, F., Tillmann, R., Wang, M. J., Wegener, R., Wildt, J., Wahner, A. and
666   Mentel, T. F.: Secondary organic aerosol formation from hydroxyl radical oxidation and
667   ozonolysis of monoterpenes, Atmos. Chem. Phys., 15, 991–1012, 2015.

668

669

670

671

672

673

674

675

676

677

Table 1: Initial conditions for the dual chamber experiments.

Exp.	Start Time (LT)	RH (%)	Temperature (°C)	BC (µg m⁻³)	OA (µg m⁻³)	% bbOA	O:C	NO (ppb)	NO₂ (ppb)	Total VOCs[b] (µg m⁻³)
1	17:45	45	17	2.4	44	70	0.4	17	24	150
2	17:45	35	13	0.8	18	65	0.36	4	22	50
3	17:50	33	15	0.6	19	37	0.25	3	20	38
4	17:55	40	14	2.5	48	68	0.33	90	20	160
5	17:45	35	15	1.1	18	69	0.4	3	25	71
6	17:50	40	17	2.6	50	72	0.36	32	25	160
7	18:00	45	20	1.0	16	78	0.36	15	20	63
8	17:55	42	22	1.2	22	77	0.45	22	22	75
9	18:15	40	19	0.7	16	75	0.44	3	14	46
10	18:15	45	21	1.6	25	50	0.33	32	21	100
11	18:30	45	24	0.6	6	48	0.41	1	5	38
12[a]	18:00	32	21	2.1	6	65	0.37	3	15	131
13[a]	18:20	30	19	3.0	33	67	0.35	31	23	188

679
680   [a] Blank experiment.
681   [b] Sum of the VOCs quantified by the PTR-MS.
682

683

684

685

686

687

688

689

690
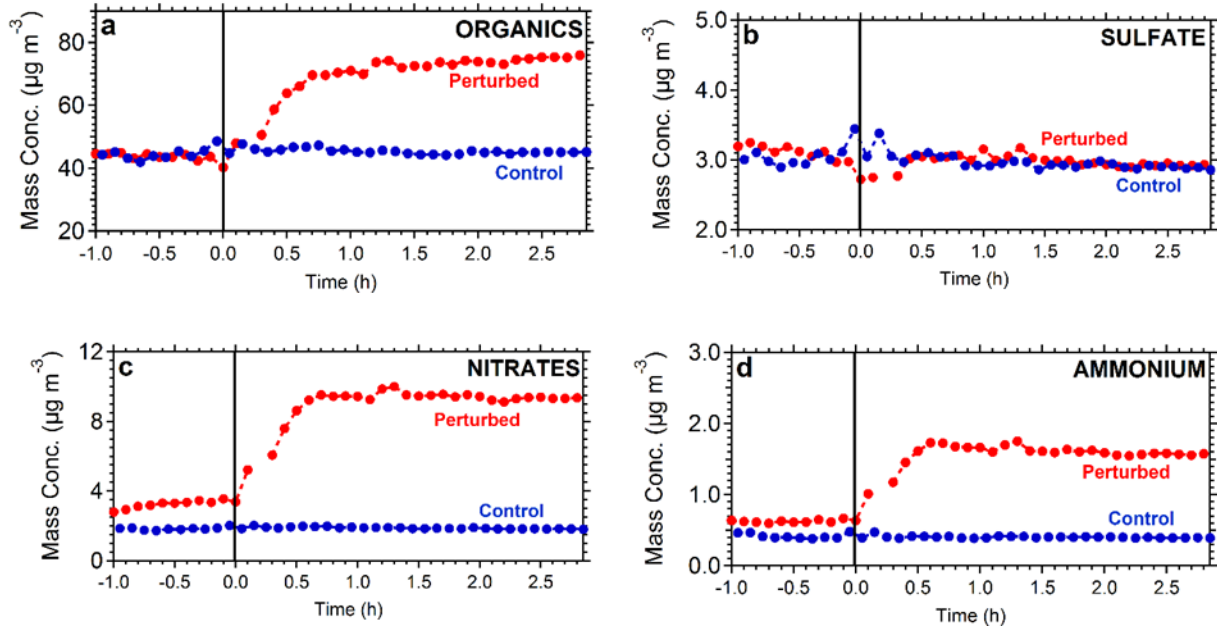
Figure 1: Particle wall-loss corrected aerosol mass concentration (CE=0.4) for the AMS-measured (a) organics, (b) sulfate, (c) nitrates, and (d) ammonium in both the perturbed (red line) and the control chamber (blue line) during Exp. 1.

694

695

696

697

698

699

700

701

702

703

704

705

706

707

708

709
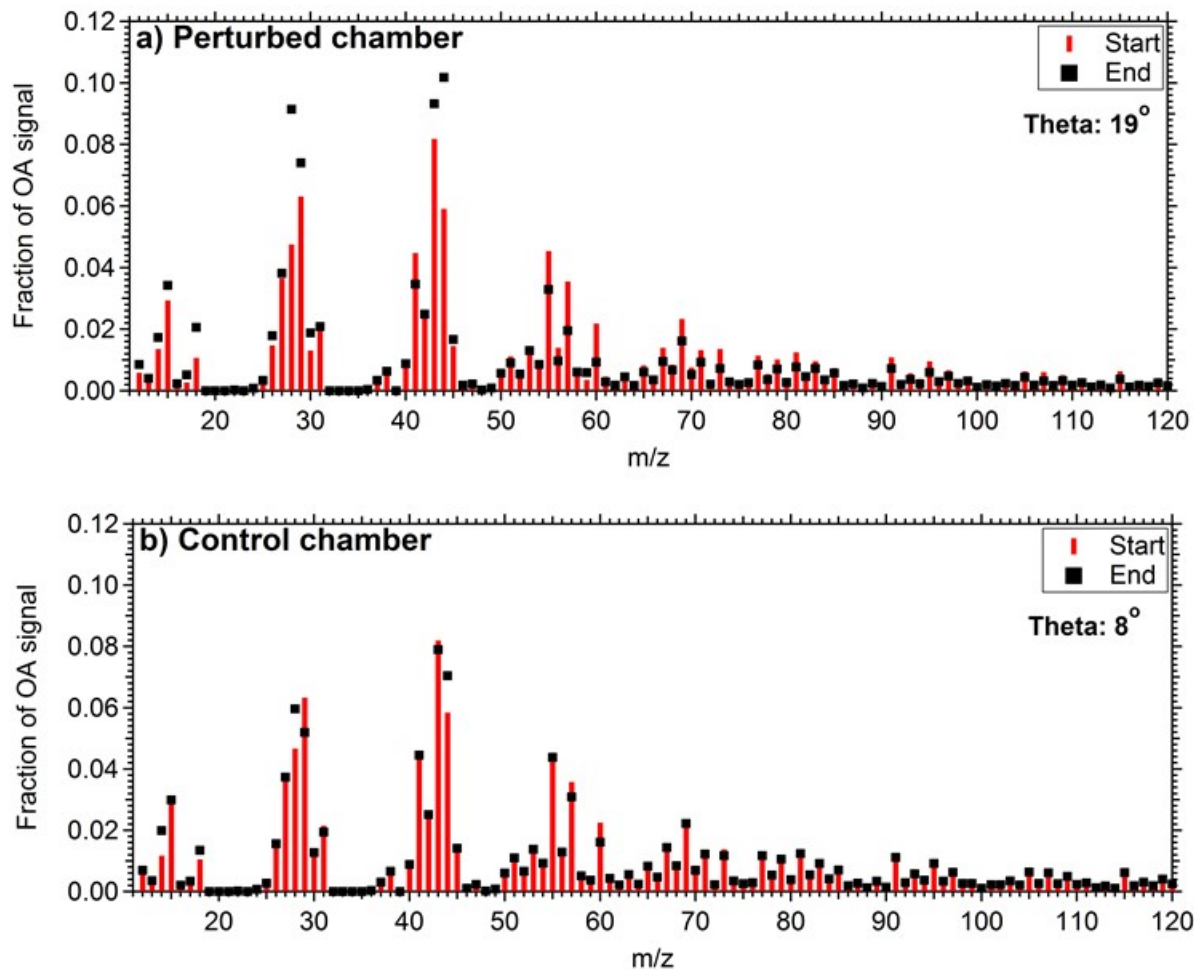
Figure 2: Mass spectra of OA during Exp. 1 in the (a) perturbed chamber and (b) control chamber

at the start of the experiment (after the filling process) and at the end of the experiment.

712

713

714

715
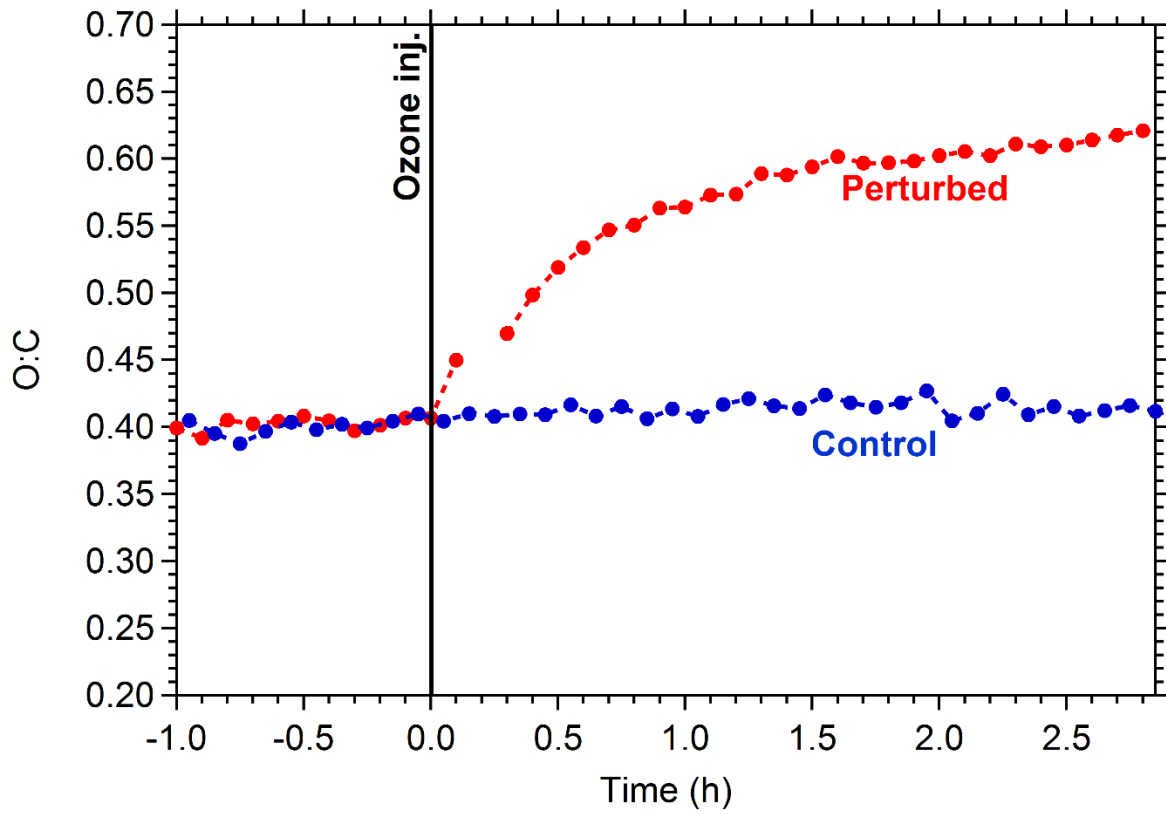
716 **Figure 3:** Oxygen to carbon ratio of the OA in the perturbed (red line) and the control chamber
717 (blue line) during Exp. 1.

718

719

720

721

722

723

724

725

726

727

728

729

730
731
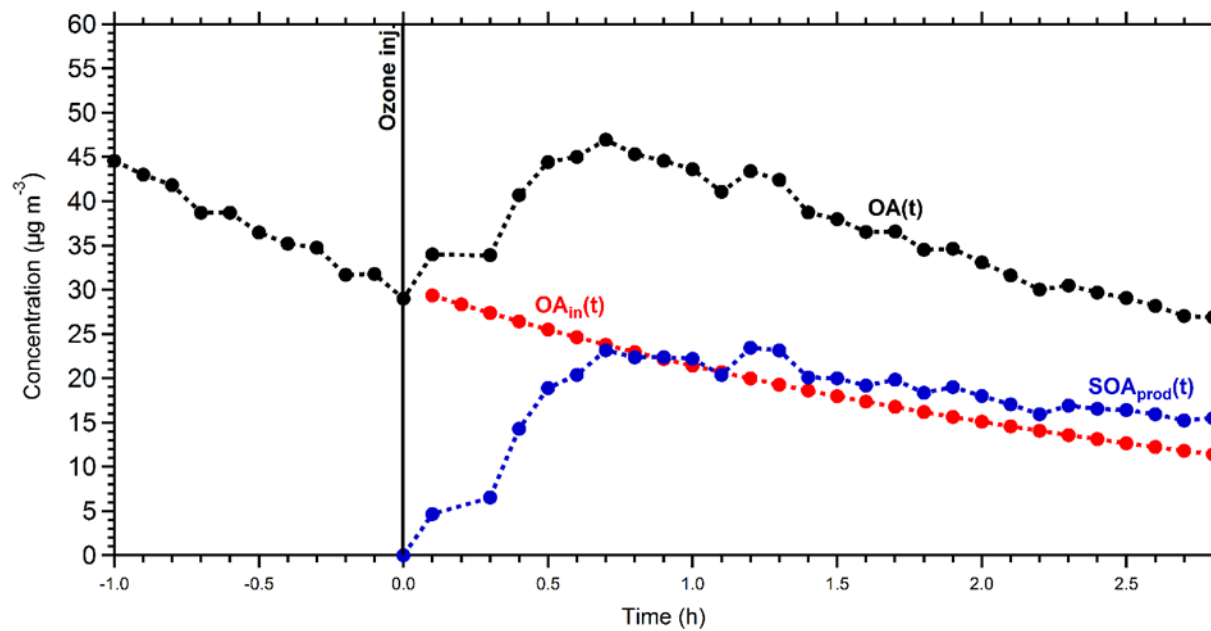
Figure 4: Mass concentration of the measured OA (black points), the initial OA (red points) and the produced SOA (blue points) in the perturbed chamber in Exp. 1. All concentrations refer to the suspended aerosol in the chamber and do not include the material deposited on the chamber walls.
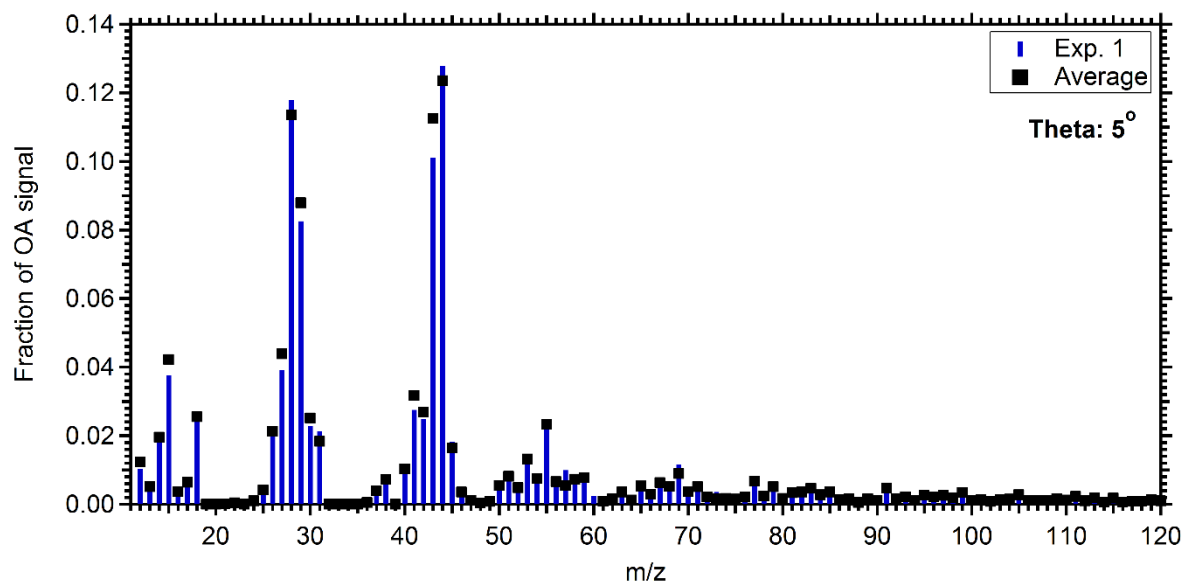
Figure 5: Mass spectrum of the produced SOA in the perturbed chamber for Exp. 1 (blue bars) and the average spectrum of the produced SOA in all experiments (black squares).

738

739

740

741

742

743

744

745

746

747

748

749

750

751

752

753

754

755

756
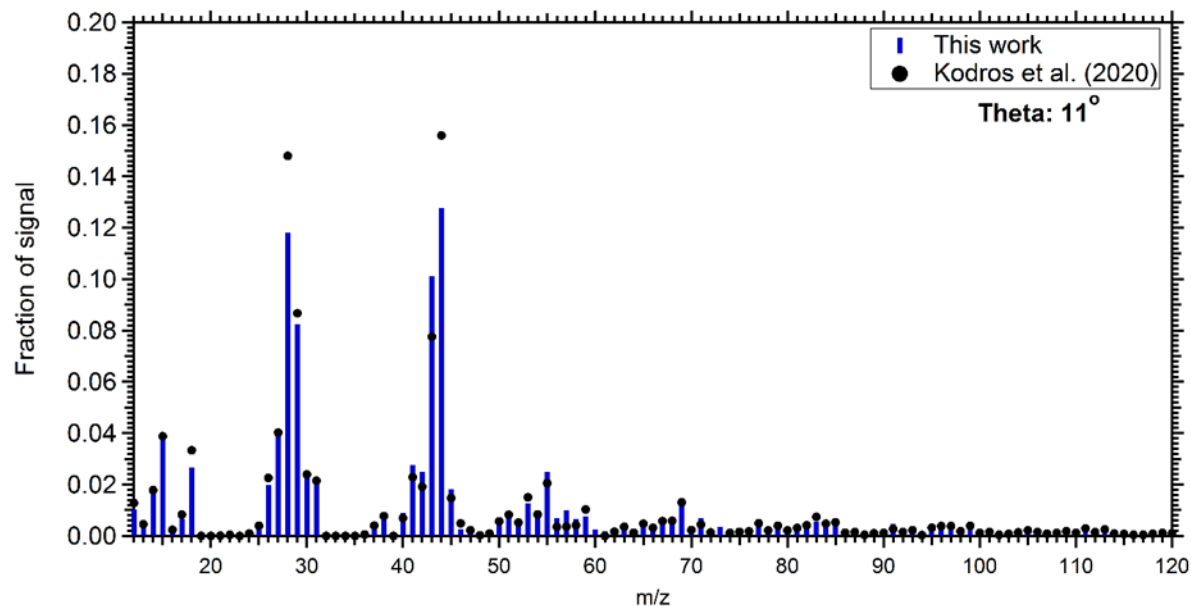
Figure 6: Comparison of the produced SOA mass spectra in the perturbed chamber during Exp. 1 (blue bars) and the produced SOA estimated during the chamber experiments of nocturnal aging of biomass burning emissions (Kodros et al. 2020) (black circles).

763

764

765

766

767

768

769

770

771

772

773

774

775

776

777
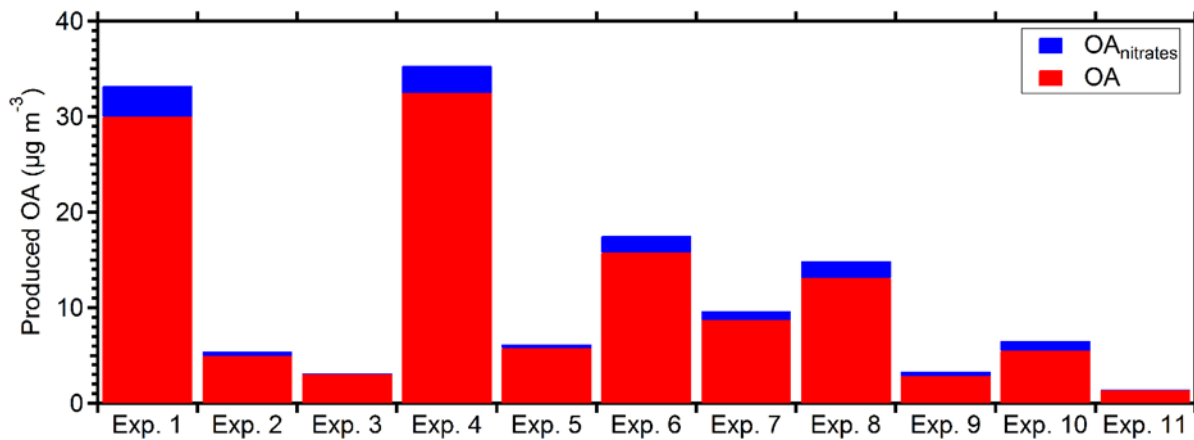
Figure 7: Produced OA (red bars) and the estimated organic nitrate (blue bars) in the perturbed chamber for the eleven perturbation experiments. All values have been corrected for wall losses and the AMS collection efficiency.

800
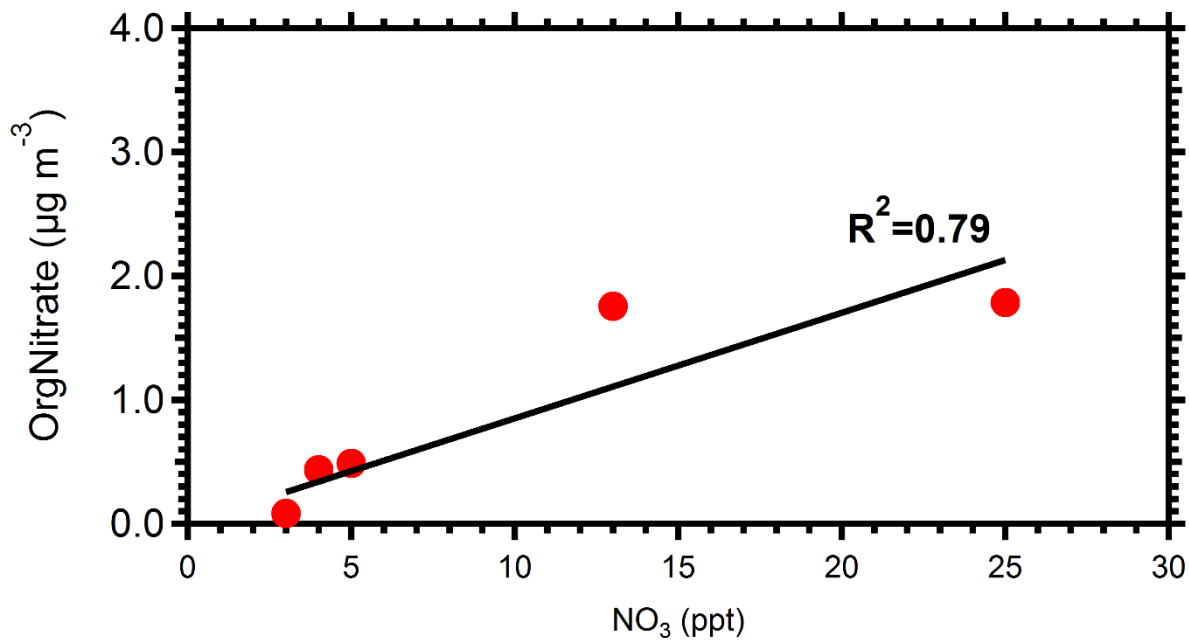
801 **Figure 8**: Correlation between NO_3 radicals with the organic nitrate formed in the perturbed

802 chamber.

803

804

805

806